CrystEngComm

Accepted Manuscript

ROYAL SOCIETY OF CHEMISTRY

www.rsc.org/crystengcomm

Journal Name

Dynamic Article Links ►

Cite this: DOI: 10.1039/c0xx00000x

www.rsc.org/xxxxxx

ARTICLE TYPE

Cucurbitural/hydroxyapatite based nanoparticles for potential use in theranostic applications

Sunita Prem Victor,[1] Willi Paul[2], Muthu Jayabalan[1] and Chandra P. Sharma[2]*

Received (in XXX, XXX) Xth XXXXXXXXX 20XX, Accepted Xth XXXXXXXXX 20XX
DOI: 10.1039/b000000x

We present the engineering of Cucurbitural/Hydroxyapatite based theranostic nanoparticles with high aspect ratio and needle shaped morphology. These particles with varying size, surface charge and tunable degradation profiles manifested advantages of cucurbitural presence with respect to drug loading, encapsulation efficacy and release kinetics. In vitro release profiles with two model drugs, Doxorubicin hydrochloride (Dox, hydrophilic) and Nile Red dye (NR, hydrophobic), were evaluated. It was ascertained that hydrophilic Dox released at a faster rate compared to hydrophobic NR for similar time periods. The concomitant presence of Samarium (Sm3+) confers theranostic potential to the synthesized nanoparticles. Cellular toxicity effects systematically assessed using MTT and live/dead assay protocols indicate inappreciable toxicity. The nanoparticles further reveal excellent blood compatibility and cellular internalization properties as visualized by fluorescence microscopy. Particles excited at 300 nm revealed Dox emission in green channel (470 nm) as well as Sm3+ emission in the red channel (590 nm) respectively. These studies unravel the potential of these nanoparticles for effective theranostic applications.

Cite this: DOI: 10.1039/c0xx00000x

www.rsc.org/xxxxxx

ARTICLE TYPE

Introduction

Non-invasive imaging represents an emerging technology that overcomes the limitations of current evaluation techniques, such as histology and biochemical assays that are intrinsically invasive, destructive and time consuming. Near-infrared (NIR) imaging offers excellent characteristics such as deep tissue penetration, minimal background fluorescence, and compatibility with existing fluorescence imaging instrumentations.[1] Recently, a multitude of nanostructures like quantum dots, silver nanoparticles, liposomes, carbon nanotubes, dendrimers, magnetic nanoparticles and calcium phosphates have been considered as potential candidates for non invasive imaging.[2-6] Conventional fluorophores like quantum dots and transition metal complexes that were widely studied as luminescent reporters are associated with limitations like low photostability and cytotoxicity. Calcium phosphates bequeathed with splendid biocompatibility properties are also known to increase brightness and the intensity of signals in the NIR range.[7] Furthermore nanoscale hydroxyapatite (HA) doped with lanthanides exhibit better fluorescence properties because of the rigid confinement of the dopant ions in the crystal lattice.[8] Lanthanide ions, functional mimics of calcium ions are found to have inappreciable toxicity *in vivo* and have immense potential for the treatment of bone density disorders.[9] In addition there lies an immediate unmet clinical need for the development of dual-acting biomaterials termed the 'theranostics' that could serve for simultaneous targeted drug delivery and fluorescence imaging guidance. Effective methods to monitor drug release kinetics are essential to foster safe, sufficient and effective therapies. Numerous nanostructured materials have been investigated for efficient imaging and therapeutic applications.[3-5] However utilization of HA based materials are of special interest due to their innate similarity with natural bone mineral.[10] In recent times, mesoporous nano HA with precise control over particle and pore distribution has been elucidated.[11, 12] HA synthesized with different morphologies including nanorods, nanocrystals, nanoparticles and nanotubes have been particularly substantiated for drug delivery applications.[13] Dual doping of HA has also been carried out to identify their potential in computer topography imaging and drug delivery.[14-16] However the well controlled synthesis of HA with desired morphology and properties for theranostic utilization still eludes us.

The subtle manipulation of structure and ideal surface functionalisation of HA could yield compatible nanoparticles with desirable attributes. Cucurbiturals are macrocyclic pumpkin shaped hexamers with partly enclosed cavity having good complexing capability with cationic and hydrophobic drugs.[17] Among the diverse kinds of cucurbiturals, cucurbituril heptahydrate (CB[7]), are being considered as ideal candidates to enhance drug loading and therapeutic efficacies due to better solubility and larger cavity size.

In this study we detail the preparation, characterization and biological evaluation of CB[7]–HA based theranostic nanoparticles. To the best of our knowledge there is limited literature available on the interactions of HA and CB[7] coupled with their potential to enhance drug loading. Herein, the concomitant presence of Samarium (Sm^{3+}) and CB[7] could unravel manifold advantages and seems to be an ideal strategy for simultaneous targeted drug delivery and fluorescence imaging guidance. The presence of CB[7] not only drastically augments loading efficiency, but also increases hydrophobicity that promotes preferred albumin adsorption. Samarium like all other lanthanides exhibit luminescence capability. The Sm^{3+} ions have a $4f^5$ configuration and are doubly degenerate for crystal field perturbation. They also possess narrow line emission profile with long lifetime and can be utilized as probes for various applications. So the presence of samarium confers theranostic capabilities to the nanoparticles. The nanoparticles of varying size and surface charge have been engineered as these are crucial for cellular internalization. Additionally morphology, structural parameters, surface area, degradation behavior, drug encapsulation efficiency, release profiles, protein adsorption, cytotoxicity by MTT and live/dead assay and cellular uptake studies of the nanoparticles have been systematically evaluated. The results indicate that these newly developed theranostic nanoparticles with tunable and sustained drug release profiles are promising fluorescent moieties for noninvasive imaging.

Experimental

Materials

CB[7] and human serum albumin was obtained from Sigma (Bangalore, India). The chemicals calcium chloride, disodium hydrogen phosphate, trisodium citrate and sodium bisulphate were procured from SD Fine Chemicals (India). Samarium carbonate was obtained from Merck (Bangalore, India). Samarium chloride was prepared by dissolving with hydrochloric acid followed by evaporating the solvent. All chemicals received were of analytical grade and were used as such without further purification. The drugs, hydrophilic Doxorubicin hydrochloride (Dox) and hydrophobic fluorescent dye Nile Red (NR) were purchased from Parenteral Drugs Ltd. (Doxopar-10, India) and Sigma (India) respectively.

Methods

The theranostic nanoparticle complexes were synthesized by a facile co-precipitation method. Preliminary studies undertaken focused on the interaction between HA and CB[7]. Different molar ratios of HA to CB[7] were initially synthesized and characterized for their phase and morphology. An optimum ratio was then selected and utilized for further modifications in the present study. Pure HA was also synthesized to compare and evaluate the properties after functionalisation with CB[7]. Typically 0.18 g of calcium chloride was dissolved in 100 ml

water. Appropriate 0.5 ml of CB[7] solution (10 mg in 1 ml) was added into the above calcium chloride solution. The pH was adjusted to 7 by using tri sodium citrate. Disodium hydrogen phosphate (2.24 g in 100 ml) and samarium chloride solutions were then introduced drop wise to the above solution mixture. The mixture was continuously agitated for 14 h. The product was filtered, washed with water, sonicated and lyophilized to obtain fine powder. The doping concentration of Sm^{3+} was varied with respect to the weight of calcium at 0, 0.2 wt% and 0.4 wt% to give different nanoparticle formulations. The formulations are hereby abbreviated as Sm0CH, Sm0.2CH and Sm0.4CH throughout the text.

Physiochemical Characterizations

The particle size (hydrodynamic radius) and surface charge (zeta potential) were determined using a Zetasizer (Malvern nanoseries, Worcestershire, UK) based on dynamic light scattering principles. Powder X-ray diffraction (XRD) patterns were obtained from a Bruker AXS, X-ray diffractometer using CuKα radiation. Scherrer formula and least square fit method were used to evaluate the average crystalline size and cell parameters respectively. Fourier transform infrared (FTIR) spectra were recorded on a Jasco FT/IR-4200 spectrophotometer. The specific surface areas of the particles were evaluated by the Brunauer–Emmett–Teller (BET) method (Quantachrome NOVA 1000e, Quantachrome, USA). The morphology of the theranostic particles were inspected by Transmission Electron Microscopy (TEM, Philips CM12 STEM, Netherlands) and Atomic Force Microscopy (AFM, alpha300A, Witec Inc., Germany) respectively. The degradation profile of the particles were evaluated by measuring the amount of calcium released at 578 nm using a calcium assay kit (Enzyme Technologies Pvt. Ltd., Baroda) in a spectrophotometer (Cary 50, Varian, USA).The *In-vitro* degradation studies of the theranostic nanoparticles was carried out by dissolution experiments in phosphate buffer(pH 7.4). Triplicate samples of 0.1 g of the nanoparticle was placed in tubes containing 50 ml of 7.4 buffer and maintained at 37^0 C. The amounts of calcium released at regular intervals of time were monitored using a Calcium Assay Kit (measured at 578nm) and the concentration was calculated as follows

Calcium Concentration= (Absorbance of test/Absorbance of Standard)*10

Luminescence excitation and emission spectra were recorded on a Hitachi F-4500 spectrophotometer. Dox and NR were selected as model drugs to determine the potential of these nanoparticles as drug delivery carriers. Drug loading, encapsulation efficiency and release studies were carried out as described previously.[18] Briefly, in a typical drug encapsulation process a known amount of dried nanoparticle was suspended in 10 ml of aqueous drug at a concentration of 25 mM for remote loading for predetermined time intervals like 2,6,12,18 and 24 h. After the specified time intervals the nanoparticle-drug complexes were separated and vaccum dried. The drug content content in the complexes was determined by suspending 50 mg in 10 ml of stimulated body fluid (pH 7.4).

Drug loading = $M_{bound}/W_{particle}$

Loading efficiency (%) = $M_{bound}/W_{theoretical}$ *100

where M_{bound} is the amount drug (mg) eluted from the particles in PBS (pH~7.4) in 24 h, $W_{particle}$ is the amount of particle (g) utilized for drug loading, and $W_{theoretical}$ is the theoretical amount of drug (mg) originally added in the reaction mixture. The amount of drug released from these nanoparticles was quantitatively measured using a UV/Vis microplate reader (Tecan, Infinite M200, Switzerland) and determined by referencing it against a standard curve.

Biocompatibility Assessments

Hemocompatibility testing was carried out to study RBC aggregation and hemolysis. Briefly, blood containing anticoagulant was centrifuged at 700 rpm to obtain RBCs and plasma. Nanoparticles (100 µg) were incubated with RBC (100 µl, diluted with PBS) for 1 h. All experiments were carried out by adding nanoparticles suspended in buffer to RBCs and results compared with identical dilution factors for the controls. Normal saline and polyethyleneimine (PEI) were used as the negative and positive controls respectively. The cells were then imaged using a phase contrast microscope (Leica DMIRB, Germany).

Hemolysis (%) was evaluated by recording the absorbance at 541nm (Varian UV–Vis spectrophotometer) as reported previously.[18] The plasma isolated was used for protein adsorption studies by discontinuous native-PAGE method of Laemmli.[19] For protein adsorption the nanoparticles (10 mg) dispersed in saline were incubated with 200 µl plasma for an hour and collected after centrifugation. The sample (20 µl) was then loaded onto the gels and separation was carried out at 100V for 90 min using Mini-PROTEAN II electrophoresis cell (Bio-Rad, CA, USA). The gels were stained with Coomassie blue and then subsequently destained in a solution containing methanol (50%) and acetic acid (10%). The gel was then imaged using an image analyzer (LAS 4000, Fuji).

Direct contact cell culture was carried out to evaluate the cytotoxicity of the prepared nanoparticles. L929 cells were seeded with DMEM medium containing 10% FBS, incubated for 24 h in 5% CO_2 and 95% humidity to attain 80% confluence. The culture medium was then removed and different concentrations of the nanoparticles were incubated for 24 h. Live/dead staining was performed using a mixture of acridine orange (100 µg/ml) and ethidium bromide (100 µg/ml) and viewed immediately under an epifluorescence microscope (Optika SRL). Fluorescence images were acquired using blue filter for acridine orange and green filter for ethidium bromide respectively. The MTT assay was performed on L929 cell line after attaining confluence as reported above. Different concentrations of the nanoparticles (10-40 µg/ml) were incubated for 24 h followed by addition of 100 µl MTT. The formazan crystals produced after medium removal were dissolved using 300 µL of DMSO and quantified measuring absorbance at 570 nm using a plate reader (Tecan, Infinite M200, Switzerland). Cellular internalization of the theranostic nanoparticles were carried out using HeLa cells seeded onto a 4-well plate with over 85% confluent growth. Nucleus was stained with DAPI followed by incubation with nanoparticle samples (2 µg/well) and drug loaded nanoparticles samples (2 µg/well) for 2 h. Post incubation the cells were washed with PBS and examined using a fluorescence microscope (Leica DMI 3000B, Germany).

Results and Discussion

The theranostic nanoparticles were facilely prepared by a simple co-precipitation technique. The morphological characteristics of the synthesized nanoparticles were evaluated using AFM and TEM. The AFM images (Figure 1a and 1b) and bright field representative TEM micrographs (Figure 1c and 1d) of HA and Sm0.2CH nanoparticle display uniform and homogenous particle size distribution and high aspect ratio particles possessing needle shaped morphology respectively. The aspect ratios calculated from the TEM software are 17.8 ± 1.8, 15.8 ± 2.1 and 7.2 ± 0.9 for Sm0CH, Sm0.2CH and Sm0.4CH nanoparticles respectively. The aspect ratio is highest for Sm0.2CH when compared to other samples containing Sm^{3+}. Higher concentrations of Sm^{3+} could not be evaluated due to solid solution formation. The TEM micrograph of Sm0.4CH nanoparticle is included as supplementary figure S1.

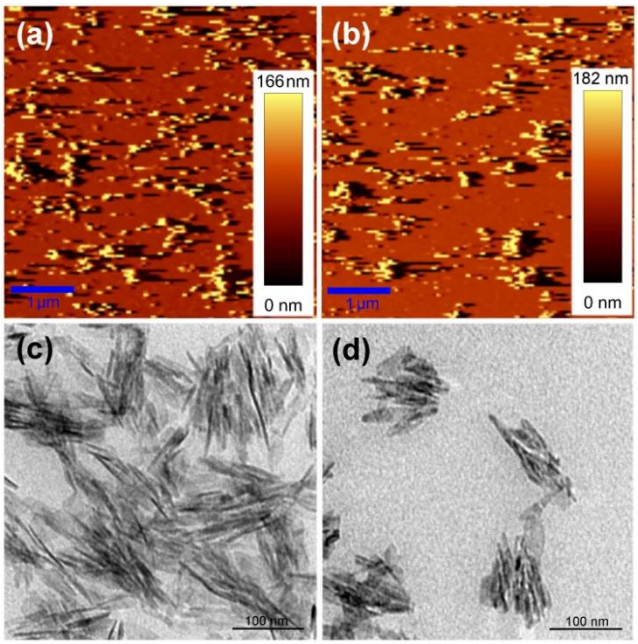

Figure 1. AFM images of (a) HA and (b) Sm0.2CH and TEM micrographs of (c) HA and (d) Sm0.2CH (b) nanoparticles respectively

The images signify that the concomitant presence of CB[7] and Sm^{3+} does not entail a change in the morphology of HA. Figure 2a represents the XRD pattern of HA, CB[7], Sm0CH, Sm0.2CH and Sm0.4CH nanoparticle respectively. The typical diffraction peaks of HA at 2θ=26.12°and 32.13° assigned to the (002) and (112) planes[20] that can be indexed to standard HA (JCPDS-09-432). CB[7] in its crystalline form exhibits peaks at 27°, 30°, 31°, 32°, 36°, 38°, 39° and 45° respectively. The diffractograms of the Sm0CH, Sm0.2CH and Sm0.4CH nanoparticles display all reflections observed for the HA phase in addition to the characteristic peaks of CB[7]. The presence of Sm^{3+} in the nanoparticles does not alter the diffraction pattern thereby confirming its inclusion in the hexagonal HA lattice. There have been concurrent reports on the inclusion of lanthanides in calcium phosphates without the detection of other phases.[14] However, the replacement of Sm^{3+} in the lattice leads to differences in the measured crystalline size and lattice parameters. The crystalline size and lattice parameters of the prepared nanoparticles Sm0CH, Sm0.2CH and Sm0.4CH are given in Table 1. An increase in concentration of Sm^{3+} results in a reduction in crystalline size. This decrease in size is attributed to the difference in charge and radius of the dopant ions which substitute at the calcium lattice sites in the hexagonal HA lattice. Parallel size measurements by DLS displayed in Table 1 also reveal a similar trend, though DLS shows larger size when compared to TEM since DLS measures the hydrodynamic radius and TEM the crystalline size. The PL emission spectra (Figure 2b) of the nanoparticles depicted that the concentration of the dopant Sm^{3+} varied the luminescence intensity, but had negligible effects on the excitation wavelength. Furthermore, dual emission for Sm^{3+} was observed at 550 nm and 660 nm, however, the PL intensity at 660 nm was relatively weaker compared to 550 nm. The emission intensity was also dependent on the concentration of drug encapsulated in the system as drug molecules induce a quenching effect on the luminescence (Figure 2c). Furthermore, the PL emission intensity of Sm^{3+} as a function of cumulative Dox release revealed that PL intensity is inversely related to the total amount of drug released.

FTIR spectra were collected to confirm that the interaction between HA and CB[7] is predominantly hydrogen bonding in nature. FTIR analysis spectrum of HA, CB[7] and Sm0CH nanoparticle is displayed in Figure 3. The IR spectrum of HA reveal peaks at 601 cm^{-1} (phosphate), 725 cm^{-1} (carbonate), 832 cm^{-1} (carbonate), 1032 cm^{-1} (phosphate), 1092 cm^{-1} (phosphate), 1384 cm^{-1} (carbonate), 1631 cm^{-1} (water) and 3400 cm^{-1} (hydroxyl). CB[7] shows characteristic peaks at 1730 cm^{-1}, 2931 cm^{-1} and 3436 cm^{-1} indicative of CO-N, C-H and C=O stretching respectively. The nanoparticles Sm0CH show the bands identical to pristine HA and CB[7]. However the characteristic carbonyl group of CB[7] shows a shift from 1730 cm^{-1} to 1720 cm^{-1} suggesting the presence of hydrogen bonding. Further the presence of carbonyls in the CB[7] exhibits coordinative interactions with the calcium of HA. This observation is concordant with iron oxide/CB[7] system evidenced in literature.[21]

To study the potential application of these nanoparticles for drug delivery we selected two model drugs, Dox and NR. The good complexation capacity of CB[7] could be instrumental in enhancing the drug encapsulation and loading potency of the nanoparticles. Besides it has been observed that there was an increase in zeta potential of the nanoparticles with an increase in Sm^{3+} concentration (Table 1). This could further promote augmentation of drug encapsulation potential. Drug loading content and encapsulation efficiency of the nanoparticles for both the selected drugs are available in Table 1. Evident enhancement has been observed for the nanoparticles for both the drugs and are in the order HA<Sm0CH<Sm0.2CH<Sm0.4CH respectively. The superior loading exhibited with NR loading when compared to Dox is explained by greater hydrophobic interaction with the CB[7] core. The primary driving force behind greater loading is the presence of CB[7] in the nanoparticles. Secondary forces like increased BET surface area and greater zeta potential of the modified nanoparticles further promote higher loading capacity (Table 1).

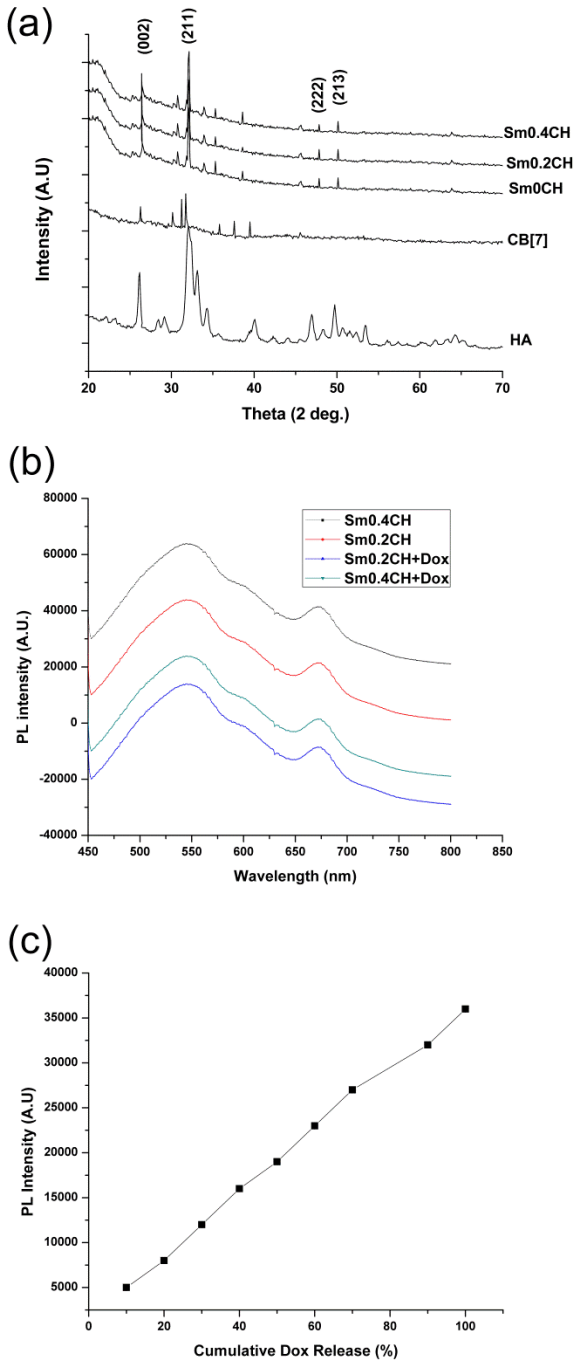

Figure 2. (a)XRD micrographs of, (b) PL spectra of Sm0.2CH and SM0.4CH nanoparticles with and without Dox loading respectively and (c) PL emission intensity of Sm^{3+}as a function of cumulative release amount of Dox from Sm0.2CH nanoparticles

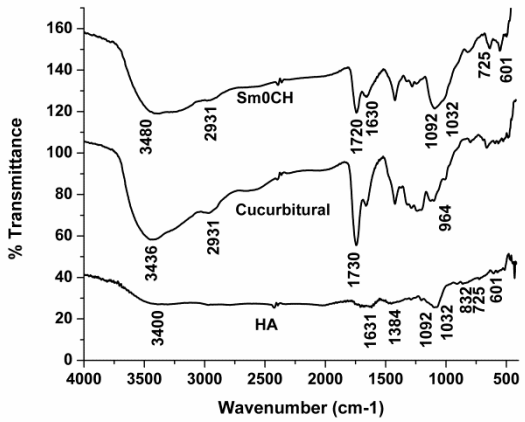

Figure 3. FTIR spectra of HA, CB[7] and Sm0CH nanoparticles respectively.

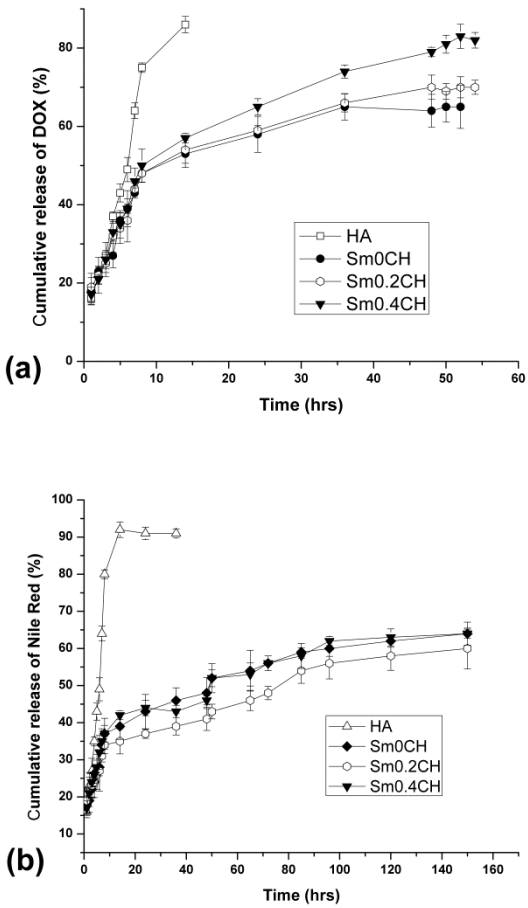

Figure 4. *In vitro* release profile of (a) Dox and (b) NR from nanoparticles at pH 7.4 respectively (SD, n=3).

Figure 4 (a and b) represents the release profile of HA and Sm0CH, Sm0.2CH and Sm0.4CH nanoparticles incubated in SBF (pH 7.4) for Dox and NR respectively. The nanoparticles in Figure 4a demonstrated a burst release within the first hour releasing around 20% of their total payload. Pure HA

nanoparticles depicted a single phase release in contrast with the other nanoparticles that followed a typical two-phase profile with an initial burst phase (1–4 h), followed by a slow and sustained release that could prolong drug effects. The uncomplexed Dox molecules adsorbed on the surface of the nanoparticle could lead to the observed drug burst. The synergistic effects of CB[7] and Sm^{3+} could be the decisive factor controlling the drug release, which resulted in subsequent sustained release for 60 h. The single phase, faster release for the HA nanoparticle mainly resulted due to faster degradation. To substantiate the drug release, preliminary degradation behavior of these nanoparticles were carried out. Around 50% of calcium was dissolved by the tenth hour for the HA nanoparticle releasing approximately 90% of loaded drug. The time increased to 15 h, 24 h and 30 h for the Sm0CH, Sm0.2CH and Sm0.4CH nanoparticles respectively. The degradation in calcium phosphates exclusively occurs by calcium detachment followed by the removal of phosphates, in which case HA will be expected to degrade rapidly as ascertained. The release profile (Figure 4b) for NR, followed a similar profile with the exception that the release was slower, gradual and more controlled. The hydrophobic NR drug exhibits a gradual and prolonged release pattern when compared to hydrophilic Dox. The cumulative release amounts of Dox from the Sm0.2CH nanoparticle were 18, 50, 56, 65 and 70% at a release time of 2, 12, 24, 36 and 48 h respectively. In contrast the release amounts of NR were 15, 22, 37, 40 and 42% for the same time period from the Sm0.2CH nanoparticle. The lesser release rate of NR can be attributed primarily to greater hydrophobic interactions with CB[7] coupled with enhanced electrostatic interactions between modified nanoparticles and NR molecules. Thus to summarise, the drug release from the nanoparticles depends on hydrophobic and electrostatic interaction between respective drug and nanoparticle. For instance the zeta potential of aqueous Dox is -20 mV and of aqueous NR is -34 mV. This high negative zeta potential of NR will result in greater electrostatic interaction with the nanoparticles when compared to Dox since the synthesised nanoparticles have positive zeta potential. Furthermore there exists a greater hydrophobic interactions with the CB[7] which results in a slower and prolonged release for NR when compared to Dox.

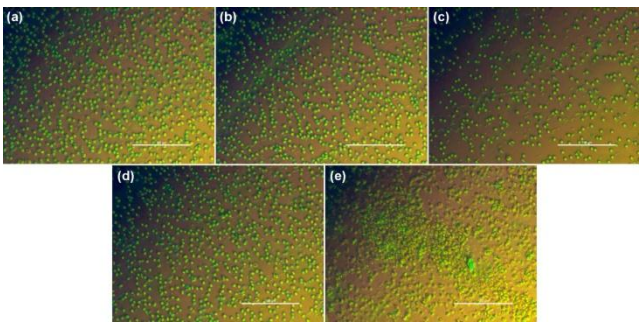

Figure 5. Micrographs of RBC aggregation experiments: (a) SM0CH, (b) Sm0.2CH, (c) Sm0.4CH, (d) negative control and (e) positive control after incubation with nanoparticles respectively.

Preliminary biocompatibility evaluation is essential to determine the suitability of synthesized nanomaterials for numerous biomedical applications. Blood cell aggregation, hemolysis and protein adsorption mediated events are limitations that can lead to serious circulatory disorders and activation of coagulation pathways.[22] Hemocompatibility of the theranostic nanoparticles were evaluated by measuring RBC aggregation and hemolysis under *in vitro* conditions. The nanoparticles did not produce any significant heamolysis (<0.5%) even at a relatively high concentration of 40 µg/ml. Moreover the images in Figure 5 illustrate that no visible aggregation was detected on incubation with RBCs and were similar to that obtained with the negative control. Thus the nanoparticles did not promote any rouleaux formation and the morphology of the cells remains intact signifying that the synthesized nanoparticles are haemocompatible.

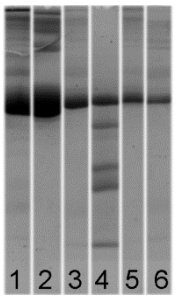

Figure 6. Demonstration of protein adsorption using PAGE :(1) Plasma, (2) Albumin Standard, (3) HA, (4) Sm0CH, (5) Sm0.2CH and (6) Sm0.4CH nanoparticles respectively

Protein adsorption by PAGE gel analysis of serum proteins obtained from the theranostic nanoparticles is shown in Figure 6. The image illustrates that there is a preferential and selective adsorption of albumin which could minimize activation of coagulation pathways.[23] The reductions in intensity of the albumin band in wells 3 to 6 indicate the selective adsorption of albumin protein. This passivation by albumin subsequently prevents fibrinogen adhesion, creating a thromboresistive nanoparticle.[24] The presence of CB[7] leads to a higher zeta potential which is instrumental in controlling the electrostatic interactions responsible for protein adsorption.[25] Moreover the concurrent presence of Sm^{3+} and CB[7] could induce a synergistic effect leading to enhanced albumin adsorption. So the Sm0.4CH nanoparticle which shows maximum albumin adsorption conceivably has the highest measured zeta potential (Table 1). These results are consistent with the preferential adsorption of albumin by nanoceria having positive zeta potential.[25]

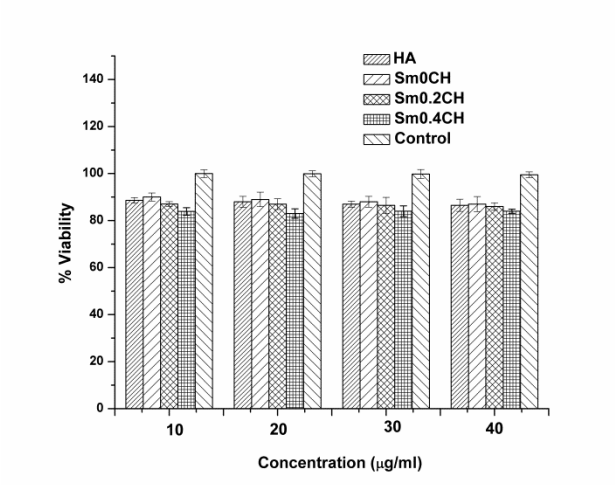

Figure 7. Cellular toxicity of the nanoparticles by MTT assay

The cellular response to the theranostic nanoparticles have been evaluated by MTT and live/dead cytotoxicity assays. Toxicity assessments are necessary to ensure safe implementation of nanomaterials. The cytotoxicity of nanoparticles is found to inherently depend on the size, shape and their interaction with cell surfaces.[26] The MTT assay results (Figure 7) demonstrated that HA, Sm0CH, Sm0.2CH and Sm0.4CH had no effect on L929 cell viability at different concentrations. In parallel the response of HeLa cells to the various nanoparticles was visualized using a fluorescence microscope. Representative images (Figure 8) are shown for the Sm0.2CH and Sm0.4CH nanoparticles respectively. A normal green fluorescence with the exception of few apoptotic cells depicts healthy cells signifying that the nanoparticles did not induce necrosis and maintained cell membrane integrity.

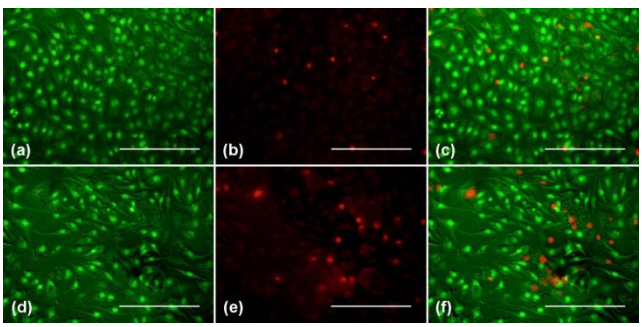

Figure 8. Live/dead images of cells incubated with nanoparticles (Live cells are represented in green and dead cells in orange). Scale bars denote 100 micron

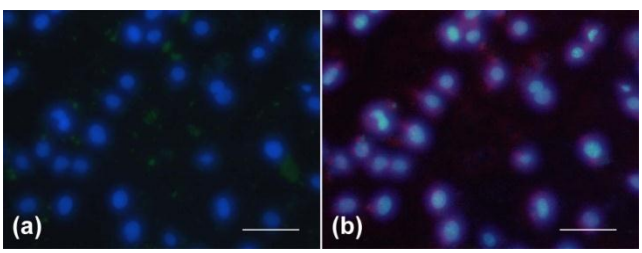

Figure 9. Internalization and excitation of nanoparticles at 300 nm on Hela cells observed by fluorescence microscopy (a) Dox emission at 470 nm and (b) Sm^{3+} emission at 590 nm. Cell nuclei are stained blue with DAPI. Scale bar denotes 100 micron

To substantiate the theranostic potential of these nanoparticles, cell uptake studies were performed using fluorescence microscopy. The intracellular uptake of nanoparticles by cells is primarily governed by two steps; an initial binding step followed by internalization.[27] The initial binding step is found to depend on the surface charge of the particle and greater uptake has been observed for positive nanoparticles when compared to their anionic counterparts.[28] Particles with higher positive charge exhibit greater affinity to cell membrane, promoted adhesion and demonstrated greater uptake. Additionally particle size plays a critical role in efficient uptake; the cut-off size by endocytosis being 200 nm.[29] The theranostic nanoparticles visualized by fluorescence microscopy (Figure 9) exhibit excellent cellular internalization after an incubation period of 2 h. The particles were excited at 300 nm and revealed DOX emission (Figure 9a) in green channel (470 nm) as well as Sm^{3+} emission (Figure 9b) in the red channel (590 nm) respectively. The nanoparticle localization unravels the fact that the particles possess optimum size and charge for efficient uptake. The uptake of nanoparticles is also a critical and necessary prerequisite for delivering advanced therapeutics into cells. Thus the results in the present study suggest that these nanoparticles possess excellent potential for simultaneous drug delivery and non-invasive imaging. Numerous tests like MTS and CKK-8 assays in addition to MTT assay are available in literature addressing the safety concerns of nanoparticles based imaging moieties for biological and imaging applications.[30-32]

Conclusions

The present study elucidates the synthesis, characterization and biological properties of cucurbitural/HA based nanoparticles for theranostic applications. The phase characterization, morphology, structural parameters, surface area and degradation behavior of the nanoparticles have been systematically evaluated by XRD, FTIR, TEM, AFM and BET measurements. The needle shaped nanoparticles were blood compatible and demonstrated inappreciable toxicity to cells *in vitro*. *In vitro* release profiles with two model drugs, hydrophilic Dox and hydrophobic NR, depicted variation in release patterns. These nanoparticles with favorable size and zeta potential demonstrated efficient cellular uptake with luminescence imaging capability.

Notes and references

[1] *Polymer Science Division, Biomedical Technology Wing, Sree Chitra Tirunal Institute for Medical Sciences & Technology, Poojappura, Thiruvananthapuram 695012, India.*
[2] *Biosurface Technology Division, Polymer Science Division, Biomedical Technology Wing, Sree Chitra Tirunal Institute for Medical Sciences & Technology, Poojappura, Thiruvananthapuram 695012, India.*
**Corresponding author: Dr. Chandra P. Sharma, E-mail: sharmacp@sctimst.ac.in*

We express our sincere thanks to The Director and Head BMT Wing, SCTIMST for the facilities provided. This work was supported by the Department of Science & Technology, Govt. of India through Fast Track Project CS-187/2011 to Dr. Sunita Prem Victor.

1. S. Selvam, K. Kundu, K. L. Templeman, N. Murthy and A. J. Garcia, *Biomaterials*, 2011, **32**, 7785-7792.
2. P. Yang, Z. Quan, C. Li, X. Kang, H. Lian and J. Lin, *Biomaterials*, 2008, **29**, 4341-4347.

3. C. Zhang, C. Li, S. Huang, Z. Hou, Z. Cheng, P. Yang, C. Peng and J. Lin, *Biomaterials*, 2010, **31**, 3374-3383.
4. C. Lai, S. Q. Tang, Y. J. Wang and K. Wei, *Mater Lett*, 2005, **59**, 210-214.
5. S. L. Gai, P. P. Yang, C. X. Li, W. X. Wang, Y. L. Dai, N. Niu and J. Lin, *Adv Funct Mater*, 2010, **20**, 1166-1172.
6. K. L. Lin, J. Chang, Y. J. Zhu, W. Wu, G. F. Cheng, Y. Zeng and M. L. Ruan, *Cryst Growth Des*, 2009, **9**, 177-181.
7. J. K. Liu, Q. S. Wu and Y. P. Ding, *Eur J Inorg Chem*, 2005, 4145-4149.
8. S. V. Dorozhkin, *Materials*, 2009, **2**, 399-498.
9. J. Zhou, Y. Sun, X. X. Du, L. Q. Xiong, H. Hu and F. Y. Li, *Biomaterials*, 2010, **31**, 3287-3295.
10. K. W. Wang, Y. J. Zhu, F. Chen and S. W. Cao, *Mater Lett*, 2010, **64**, 2299-2301.
11. W. Amer, K. Abdelouahdi, H. R. Ramananarivo, M. Zahouily, A. Fihri, K. Djessas, K. Zahouily, R. S. Varma and A. Solhy, *Crystengcomm*, 2014, **16**, 543-549.
12. W. Amer, K. Abdelouandi, H. R. Ramananarivo, M. Zahouily, A. Fihri, Y. Coppel, R. S. Varma and A. Solhy, *Mater Lett*, 2013, **107**, 189-193.
13. M. Itokazu, W. Y. Yang, T. Aoki, A. Ohara and N. Kato, *Biomaterials*, 1998, **19**, 817-819.
14. F. Chen, P. Huang, Y. J. Zhu, J. Wu, C. L. Zhang and D. X. Cui, *Biomaterials*, 2011, **32**, 9031-9039.
15. A. C. Queiroz, J. D. Santos and F. J. Monteiro, *Key Eng Mat*, 2005, **284-286**, 407-410.
16. S. P. Victor and T. S. Kumar, *J. Biomed. Nanotechnol.*, 2008, **4**, 203-209.
17. J. Lagona, P. Mukhopadhyay, S. Chakrabarti and L. Isaacs, *Angew Chem Int Ed Engl*, 2005, **44**, 4844-4870.
18. S. P. Victor and C. P. Sharma, *Colloids Surf B Biointerfaces*, 2013, **108**, 219-228.
19. U. K. Laemmli, *Nature*, 1970, **227**, 680-685.
20. N. Rameshbabu, K. P. Rao and T. S. Kumar, *J Mater Sci*, 2005, **40**, 6319-6323.
21. F. Benyettou, I. Milosevic, Y. Lalatonne, F. Warmont, R. Assah, J. C. Olsen, M. Jouaid, L. Motte, C. Platas-Iglesias and A. Trabolsi, *J Mater Chem B*, 2013, **1**, 5076-5082.
22. K. Kottke-Marchant, J. M. Anderson, Y. Umemura and R. E. Marchant, *Biomaterials*, 1989, **10**, 147-155.
23. J. Ji, L. Feng and M. A. Barbosa, *Biomaterials*, 2001, **22**, 3015-3023.
24. M. Amiji and K. Park, *Biomaterials*, 1992, **13**, 682-692.
25. S. Patil, A. Sandberg, E. Heckert, W. Self and S. Seal, *Biomaterials*, 2007, **28**, 4600-4607.
26. K. Y. Win and S. S. Feng, *Biomaterials*, 2005, **26**, 2713-2722.
27. C. Wilhelm, C. Billotey, J. Roger, J. N. Pons, J. C. Bacri and F. Gazeau, *Biomaterials*, 2003, **24**, 1001-1011.
28. M. R. Lorenz, V. Holzapfel, A. Musyanovych, K. Nothelfer, P. Walther, H. Frank, K. Landfester, H. Schrezenmeier and V. Mailander, *Biomaterials*, 2006, **27**, 2820-2828.
29. C. He, Y. Hu, L. Yin, C. Tang and C. Yin, *Biomaterials*, 2010, **31**, 3657-3666.
30. M. Nyk, R. Kumar, T. Y. Ohulchanskyy, E. J. Bergey and P. N. Prasad, *Nano Lett*, 2008, **8**, 3834-3838.
31. H. Y. Xing, X. P. Zheng, Q. G. Ren, W. B. Bu, W. Q. Ge, Q. F. Xiao, S. J. Zhang, C. Y. Wei, H. Y. Qu, Z. Wang, Y. Q. Hua, L. P. Zhou, W. J. Peng, K. L. Zhao and J. L. Shi, *Sci Rep-Uk*, 2013, **3**.
32. L. Q. Xiong, T. S. Yang, Y. Yang, C. J. Xu and F. Y. Li, *Biomaterials*, 2010, **31**, 7078-7085.

Table 1: Characterization of DLS size, zeta potential, crystalline size, surface area, cell parameters and drug loading capacity of HA, Sm0CH, Sm0.2CH and Sm0.5CH nanoparticles

Sample	DLS Size (Z- Average) (nm)	PDI	Zeta Potential (mV)	DOX Loading Capacity (mg/g)	Nile Red Loading Capacity (mg/g)	Crystalline Size (nm)	Surface area (m^2/g)	Cell Parameters (nm)
HA	110±2.3	0.13	-25	250	140	28	32.63	a = b = 0.9413, c = 0.6879
Sm0CH	150±0.6	0.19	-12	380	540	32	52.61	a = b = 0.9413, c = 0.6879
Sm0.2CH	130±2.3	0.16	+8	430	590	30	63.23	a = b = 0.9416, c = 0.6880
Sm0.4CH	110±0.3	0.23	+12	540	720	25	73.67	a = b = 0.9420, c = 0.6882

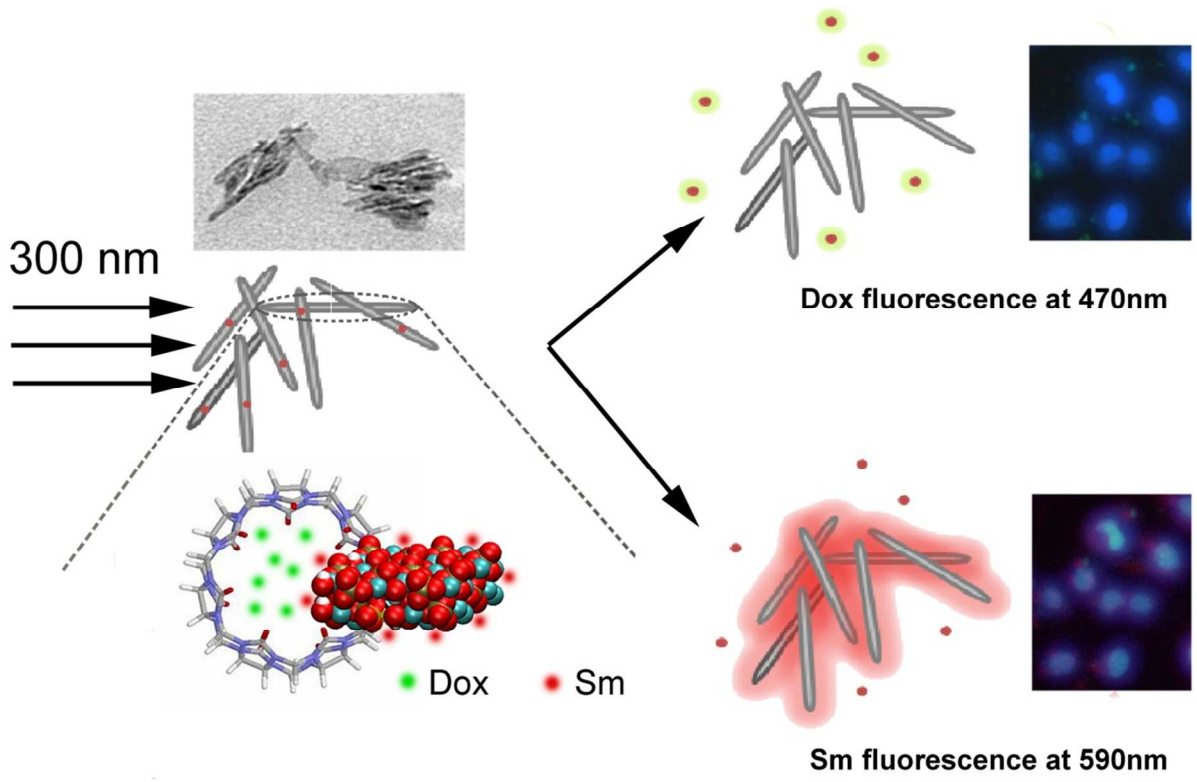

Interactions of cucurbitural and hydroxyapatite augment drug loading and concomitant presence of Samarium confers theranostic potential.